The 108M Polymorph of Human Catechol *O*-Methyltransferase Is Prone to Deformation at Physiological Temperatures†

Karen Rutherford,‡ Brian J. Bennion,§,|| William W. Parson,*,‡ and Valerie Daggett*,‡,||

Departments of Biochemistry and Medicinal Chemistry, University of Washington, Seattle, Washington 98195-7610

Received September 30, 2005; Revised Manuscript Received December 12, 2005

ABSTRACT: The human gene for catechol *O*-methyltransferase (COMT) contains a common polymorphism that results in substitution of methionine (M) for valine (V) at residue 108 of the soluble form of the protein. While the two proteins have similar kinetic properties, 108M COMT loses activity more rapidly than 108V COMT at 37 °C. The cosubstrate *S*-adenosylmethionine (SAM) stabilizes the activity of 108M COMT at 40 °C. The 108M allele has been associated with increased risk for breast cancer, obsessive-compulsive disorder, and aggressive and highly antisocial manifestations of schizophrenia. In the current work, we have constructed homology models for both human COMT polymorphs and performed molecular dynamics simulations of these models at 25, 37, and 50 °C to explore the structural consequences of the 108V/M polymorphism. The simulations indicated that replacing valine with the larger methionine residue led to greater solvent exposure of residue 108 and heightened packing interactions between M108 and helices α2, α4 (especially with R78), and α5. These altered packing interactions propagated subtle changes between the polymorphic site and the active site 16 Å away, leading to a loosening of the active site. At physiological temperature, 108M COMT sampled a larger distribution of conformations than 108V. 108M COMT was more prone to active-site distortion and had greater overall, and SAM binding site, solvent accessibility than 108V COMT at 37 °C. Similar structural perturbations were observed in the 108V protein only at 50 °C. Addition of SAM tightened up the cosubstrate pocket in both proteins and prevented the altered packing at the polymorphic site in 108M COMT.

Catechol *O*-methyltransferase (COMT,[1] E.C. 2.1.1.6) catalyzes the transfer of a methyl group from *S*-adenosylmethionine (SAM) to the phenolic hydroxyl group of catechol substrates and is involved in the catabolism of catechol estrogens and the catecholamine neurotransmitters dopamine, epinephrine, and norepinephrine (*1*−*3*). The gene encoding COMT has been localized to chromosome 22 band q11.2 (*4*, *5*). Separate promoters enable the expression of two COMT isozymes from this locus: a 221-residue soluble form (COMT in this paper) and a 271-residue membrane-bound form (MB-COMT) containing an additional 50 residues at the N-terminus (*6*, *7*). COMT and MB-COMT have similar mechanisms, requirements for Mg^{2+}, pH optima, and K_Ms for SAM (*2*). However, they have different substrate preferences, with MB-COMT exhibiting a much higher affinity for neurotransmitters such as dopamine and norepinephrine than COMT (*3*, *8*). COMT is cytosolic and is expressed abundantly in the liver and kidneys, while MB-COMT is microsomal and is the predominant form in the brain and adrenal medulla (*9*, *10*).

COMT is a member of the SAM-dependent methyltransferase fold family. Despite divergent sequences, the structural homology of this ∼135-member family is remarkably conserved (*11*, *12*). All enzymes of this family share a central seven-stranded mixed β-sheet sandwiched between two layers of α-helices (Figure 1). Crystal structures of rat COMT with bound substrate analogues reveal a single-domain α/β protein consisting of the conserved fold, with an elongated loop between β6 and β7 (the catalytic loop) forming part of the catechol binding site, and three additional helices (α1, α2, and α6) (Figure 1) (*13*−*15*). SAM, Mg^{2+}, and the catechol substrate bind to shallow clefts on the protein surface. Human and rat COMT share 81% sequence identity, and the residues involved in SAM and Mg^{2+} binding are strongly conserved. No high-resolution structures have been described for human COMT.

The human *COMT* gene has a common single nucleotide polymorphism (SNP) that results in the substitution of methionine for valine at residue 108 (*16*−*18*). Approximately 25% of the United States Caucasian population is homozygous for the 108M allele (*19*, *20*). Although the purified forms of 108V and 108M human COMT have similar kinetic properties (*8*, *21*), individuals homozygous for the 108M allele have 2−4-fold lower enzyme activity in erythrocytes,

† Financial support for this work was provided by the National Institutes of Health (Grant GM 50789 to V.D.) and the Canadian Institutes of Health (DRA to K.R.).

* Corresponding authors. V.D.: e-mail, daggett@u.washington.edu. W.W.P.: e-mail, parsonb@u.washington.edu.

‡ Department of Biochemistry, University of Washington.

§ Present address: Biosciences Directorate, Lawrence Livermore National Laboratory, Livermore, CA 94550.

|| Department of Medicinal Chemistry, University of Washington.

[1] Abbreviations: COMT, catechol *O*-methyltransferase; SAM, *S*-adenosylmethionine; SNP, single nucleotide polymorphism; T_{50}, temperature resulting in 50% inactivation; VCFS, velocardiofacial syndrome; MD, molecular dynamics; Cα-RMSD, Cα root-mean-square deviation from the starting structure; Cα-RMSF, Cα root-mean-square fluctuation about the mean structure; SASA, solvent-accessible surface area.

10.1021/bi051988i CCC: $33.50
Published on Web 01/31/2006

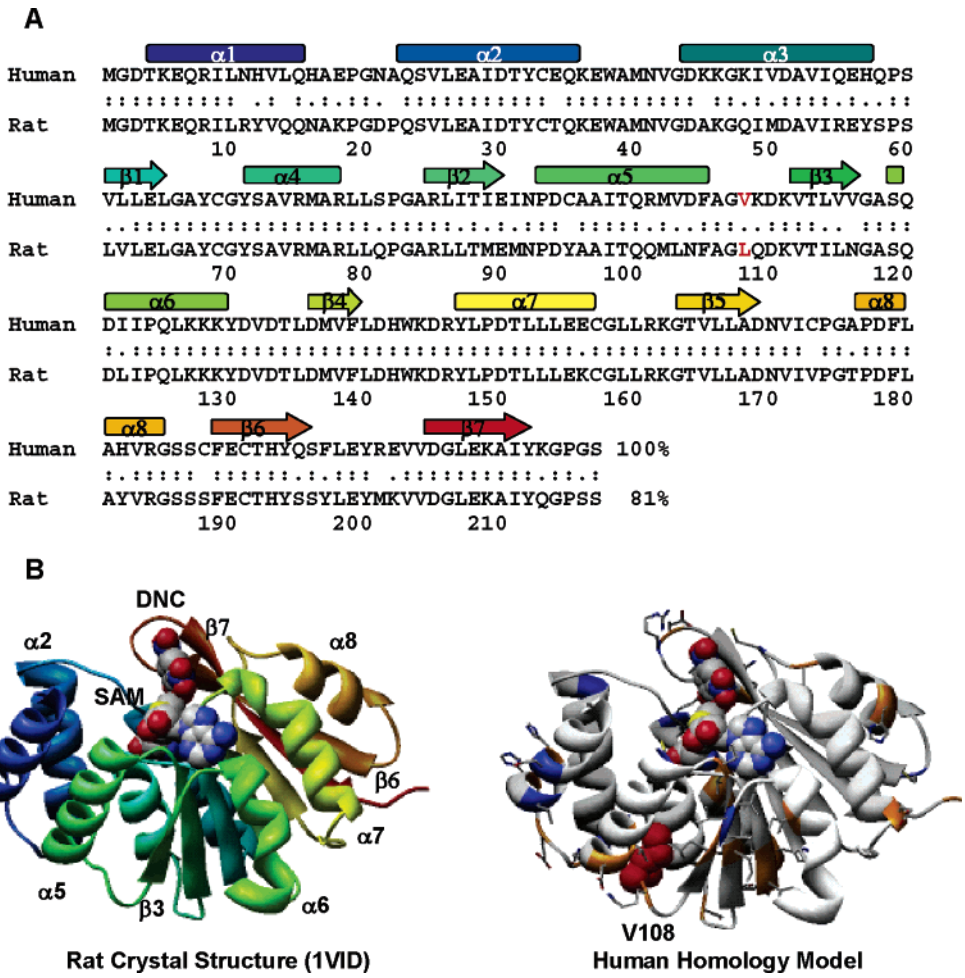

FIGURE 1: The human COMT homology model. (A) The alignment of human and rat COMT sequences was made using LALIGN (*74*). α-Helices and *β*-strands are denoted by bars and arrows, respectively, and are colored to match the ribbon representation of rat COMT. Conserved residues and conservative substitutions are denoted by (:) and (.). (B) Ribbon diagrams of rat COMT (1VID, *13*) and the human homology model. Rat COMT is colored from blue (N-terminus) to red (C-terminus). Residues replaced to create the human COMT model are colored in orange (conservative) and blue (nonconservative). The polymorphic residue 108 is colored in red. SAM and 3,5-dinitrocatechol (DNC) are shown in space-filling representation and colored by atom.

lymphocytes, liver biopsy extracts, and post-mortem dorsolateral prefrontal cortex tissues than those homozygous for the 108V allele (*22*−*28*). This difference has been ascribed primarily to a lower thermal stability of the 108M protein (*8*, *22*−*30*). Shield et al. reported T_{50} (temperatures resulting in 50% inactivation) values of 53.7 ± 0.1 and 49.7 ± 0.3 °C for the 108V and 108M proteins, respectively (*28*). SAM has been found to stabilize the activity of 108M COMT at 40 °C (*8*). Recent studies have indicated that 108M COMT is more susceptible to inactivation through oxidation than the 108V protein (*31*, *32*). These kinetic and thermal stability data imply that position 108 is important for COMT activity and that 108V and 108M COMT may differ structurally. In addition, a haplotype involving polymorphisms at position 108 and several noncoding sites has been reported to affect COMT mRNA levels (*33*, *34*); however, one recent study found no such effects (*22*).

Residue 108 is located approximately 16 Å from the active site in a loop between α5 and *β*3, both of which have SAM binding residues at their distal ends (Figure 1). Phylogenic analyses demonstrate conservation of a leucine residue at position 108 in most species, while primates have a valine at this position. Chen et al. recently created L108V mutants of mouse COMT to examine the effects of residue 108 on enzyme activity (*22*). Interestingly, replacing leucine 108 by valine resulted in a drastic reduction of COMT activity compared with the L108 wild-type protein at 37 °C, suggesting a possible evolutionary trend toward decreased activity.

The 108M allele has been associated with increased risk for breast cancer (*21*, *35*−*37*), obsessive-compulsive disorder (*38*), rapid-cycling bipolar disorder (*39*−*41*), adult-onset alcoholism (*42*−*44*), and aggressive and highly antisocial manifestations of schizophrenia (*45*−*49*). However, in the general population, a particular haplotype involving the 108V allele and two additional noncoding *COMT* SNPs was recently shown to be strongly associated with bipolar disorder and schizophrenia (*33*, *50*−*52*). 108M COMT appears to be strongly linked to neuropsychiatric dysfunction in velocardiofacial syndrome (VCFS), a chromosomal disorder resulting from a deletion of multiple contiguous genes, including *COMT*, from the long arm of chromosome 22 (*53*−*55*). Individuals with VCFS who are hemizygous for the 108M allele may suffer from elevated levels of dopamine in the brain due to decreased clearance of the neurotransmitter (*53*, *54*). Interestingly, the 108M allele has also been linked to increased sensitivity to pain (*56*, *57*) and improvement in

prefrontal cognitive function, especially working memory (*58*, *59*).

Previous computational studies of rat COMT have dealt mainly with the mechanisms of catechol binding and methyl transfer (*60*−*66*). Quantum mechanical and semiempirical calculations in vacuo by Bruice and co-workers have focused on the geometries of ground and putative transition states in COMT catalysis (*60*−*63*). The activation free energy of catalysis has been described using molecular dynamics (MD) simulations and quantum mechanical free energy calculations (*64*, *65*). While these studies have contributed to the understanding of methyltransferase catalysis, the issue of how structural perturbations caused by the introduction of methionine at position 108 results in the observed decrease in thermal stability has not been addressed. Accordingly, we have built homology models of human 108V and 108M COMT and performed multiple MD simulations of these models at 25, 37, and 50 °C in the presence and absence of SAM. The simulations showed that 108M COMT was more prone to exist in deformed conformations at physiological temperature. Altered hydrophobic packing around the polymorphic M108 residue enhanced susceptibility to increases in the solvent accessibility of the overall protein and the SAM binding site ~16 Å away. Similar structural perturbations also occurred in 108V COMT, but only at 50 °C. The addition of SAM decreased the solvent accessibility of the overall protein and the SAM binding site and minimized secondary structure reorientations throughout both COMT proteins at physiological temperatures. The stabilizing effect of SAM was less evident for 108M COMT at 50 °C.

METHODS

Homology Model. An initial homology model of human 108V COMT was generated from a 2 Å crystal structure of rat COMT (1VID, residues 4−216), which shares 81% sequence identity with the human protein (Figure 1) (*13*). The side chains of the nonidentical rat residues were replaced sequentially using a Monte Carlo procedure that minimized the torsional, electrostatic, and van der Waals energies of each residue (*67*). Two passes through the sequence were completed so that residues altered early in the sequence could rearrange in response to later modifications. Altogether, 40 residues were changed, including 30 conservative replacements (Figure 1). The model of 108M COMT was generated from the 108V homology model by replacing Val 108 with Met and minimizing the torsional, electrostatic, and van der Waals energies of the resultant structure in vacuo. A model of human 108L COMT was also created to study the effects of residue identity and size at position 108 on overall COMT structure and dynamics. Leucine was chosen because it is intermediate in size between valine and methionine and because single mutations of leucine to valine and methionine in mouse COMT affect activity (*22*).

S-Adenosylmethionine Model. The *S*-adenosylmethionine model was constructed using the atomic coordinates of SAM from the rat crystal structure (1VID, *13*). Atomic partial charges and potential function parameters were taken from the ENCAD parameter library [Supporting Information, Table S1 (*68*)].

Molecular Dynamics Simulations. Molecular dynamics (MD) simulations of the 108V and 108M COMT homology models were performed with and without SAM; simulations of the 108L COMT homology model were performed without SAM. Additionally, multiple MD simulations of the rat apoprotein (1VID, *13*) were run to serve as a control of model stability. SAM was treated as part of the protein for minimization and dynamics purposes but was not covalently bound to the protein. Simulations of the apo- and SAM-bound proteins were performed with the *il*mm (*69*) and ENCAD (*70*) simulation packages using protocols described elsewhere (*68*−*72*). *il*mm utilizes the same potential function and integration algorithms as ENCAD and is a scalable parallel molecular mechanics kernel currently used for all simulations in the Daggett laboratory. Briefly, the simulations included all hydrogens and explicit flexible three-center waters (*71*). The proteins were solvated in a rectangular box with walls extending at least 10 Å from any protein atom. The solvent density was set to 0.997, 0.993, and 0.988 g/mL for simulations performed at 25, 37, and 50 °C, respectively (*73*). A 10 Å cutoff range was used for nonbonded interactions, and the nonbonded interaction pair list was updated every three (*il*mm) to five (ENCAD) steps. The potential energy functions as implemented in *il*mm and ENCAD were used to propagate MD trajectories in the microcanonical ensemble (NVE) (*68*−*72*). A time step of 2 fs was used in all calculations, and structures were saved every 0.2 (ENCAD) to 1.0 (*il*mm) ps for analysis. Multiple 20−30 ns simulations of each apoprotein system were performed at 25 ($n = 2$), 37 ($n = 2$), and 50 °C ($n = 3$), yielding approximately 150000 structures per trajectory.

Analysis. Average Cα-RMSDs, Cα-RMSFs, contact distances, and solvent-accessible surface areas (SASA) were calculated using structures from the last 5 ns of each simulation. A contact was defined as a C−C atom distance within 5.4 Å or a heavy atom (O, N, S) distance within 4.6 Å in two nonneighboring residues. Solvent-accessible surface areas were determined using in-house software implementing the NACCESS algorithm (*75*). SAM was removed from structures that included it prior to calculating average solvent accessibilities. The errors and distributions described in Tables 1, 2, and S2 and Figure 6 are based on sets of two simulations at both 25 and 37 °C and three simulations at 50 °C for the COMT apoproteins. The errors are based on the standard deviations in the average values of the ensembles at each temperature. In Figure 2, Cα-RMSF values for the rat holoprotein (1VID, *13*) were calculated from the crystallographic *B*-factors using Cα-RMSF = $[3(B\text{-factor})/(8\pi^2)]^{1/2}$ (*76*). Figure images were generated using Chimera (*77*).

RESULTS AND DISCUSSION

Simulations of the COMT Apoprotein. As the MD simulations of human COMT described here are based on homology models, we monitored the root-mean-square deviations of the Cα atoms (Cα-RMSD) from their positions in the starting structures as a general measure of stability. Although 20% of the amino acid side chains (40 residues) were altered to build the homology models, the Cα-RMSD between the model of human 108V COMT and the rat crystal structure (1VID, *13*) was less than 0.5 Å after initial minimization. The Cα-RMSD between the 108V and 108M COMT starting structures was 0.1 Å after minimization. At 25 °C, all of the apoprotein homology models reached average Cα-RMSDs

Table 1: General Properties of the Simulations

protein	temp (°C)	Cα-RMSD (Å)	W38 (Cγ)−P174 (Cγ) distance (Å)	solvent-accessible surface area (Å^2)		
				total	SAM site[a]	catechol site[b]
108V apoprotein	initial	0.0	11.8	9038	747	623
	25	2.2 ± 0.3	14.1 ± 0.8	10356 ± 114	1121 ± 160	676 ±79
	37	2.7 ± 0.4	19.6 ± 1.4	10855 ± 143	1316 ± 203	848 ± 107
	50	3.2 ± 1.1	25.3 ±1.3	11166 ± 149	1368 ± 222	1128 ± 120
108M apoprotein	initial	0.0	11.5	9018	746	620
	25	2.2 ± 0.4	19.2 ± 1.1	10605 ± 116	1275 ± 208	893 ± 109
	37	3.0 ± 0.8	21.3 ± 0.9	11000 ± 134	1493 ± 243	909 ± 168
	50	3.3 ± 1.3	23.4 ± 1.5	11082 ± 167	1373 ± 177	1029 ± 133
108L apoprotein	initial	0.0	11.6	9415	781	640
	25	2.2 ±0.4	16.8 ±0.8	10794 ± 128	1138 ± 156	773 ± 95
	37	2.3 ± 0.2	20.1 ± 1.2	10690 ± 125	1325 ± 48	1022 ± 124
	50	3.3 ± 1.3	19.3 ± 1.1	11359 ± 173	1448 ± 236	1034 ± 166
108V + SAM	initial	0.0	11.6	9092	783	604
	25	1.8 ± 0.1	17.8 ± 0.5	10421 ± 126	1029 ± 119	850 ±95
	37	1.9 ± 0.1	17.1 ± 0.6	10482 ± 152	1136 ± 156	690 ± 88
	50	1.8 ± 0.1	13.4 ± 0.7	10393 ± 169	1042 ± 167	713 ± 125
108M + SAM	initial	0.0	11.7	9042	787	597
	25	2.1 ± 0.1	14.2 ± 0.6	10385 ± 100	1085 ± 124	809 ± 76
	37	1.8 ± 0.1	15.2 ± 0.8	10593 ± 159	1213 ± 225	832 ± 208
	50	3.8 ± 0.1	19.1 ± 1.0	11146 ± 152	1276 ± 154	1099 ± 127

[a] The SAM binding site (Å^2) was defined using the following residues: A39, M40, N41, V42, E64, L65, G66, A67, Y68, G70, Y71, S72, I89, E90, I91, N92, C95, G117, A118, S119, Q120, F139, D141, H142, W143, K144, R146, and D150. Calculations used structures from the last 5 ns of each simulation. [b] The average SASA for the catechol binding site (Å^2) was calculated as described above using the following residues: W38, M40, K46, D141, K144, D169, N170, C173, P174, L198, E199, Y200, R201, and D205.

of 2.2 Å (Table 1). These deviations were due mainly to the large number of loops in the protein (Figure 1B) rather than to instability of the homology models: the rat protein behaved similarly during simulations at 25 °C (data not shown) and the Cα-RMSDs in regions of the protein with α-helix and β-strand secondary structure were only 0.5 Å.

Figure 2 shows the Cα root-mean-square fluctuations (Cα-RMSF) about the mean structure for all the simulations, along with crystallographic *B*-factors of rat COMT with bound SAM and 3,5-dinitrocatechol (DNC) (1VID, *13*). At 25 and 37 °C, the fluctuations per residue for the rat apoprotein were essentially superposable and followed the same general pattern as the *B*-factors of 1VID, but were ∼1.5 times greater in magnitude (Figure 2A). The larger Cα-RMSFs are due to the increased dynamics of rat COMT in solution compared to the crystallized protein, while the similarities in fluctuations indicate that the rat apoprotein simulations are stable and suitably depict COMT dynamics. At 25 °C, the fluctuations per residue for all homology models followed the same pattern and were of the same magnitude as those of the rat apoprotein (Figure 2A−D). The largest Cα-RMSFs were observed in the helices and loops of the protein, especially α1, α2, α5−α8, and the catalytic loop (residues 198−205) between β6 and β7. Strands within the β-sheet core demonstrated the smallest fluctuations (Figure 2A−D). Simulations of 108V COMT showed a trend of increasing Cα-RMSDs with temperature (Table 1). The Cα-RMSD of 108M COMT increased more abruptly at 37 °C, reaching 3.0 ± 0.8 Å. Helices α6−α8 of 108M COMT showed a significant increase in the overall fluctuations per residue between 25 and 37 °C and little additional increase at 50 °C (Figure 2D). This abrupt disordering was not observed in 108V or 108L COMT, where the average Cα-RMSFs at 37 °C were intermediate between those at 25 and 50 °C (Figure 2B,C).

Residue 108 is located in a short, stable loop between α5 and β3, ∼16 Å from the SAM binding site (Figures 1 and 3). In the initial structures of both 108M and 108V COMT, residue 108 forms contacts with residues in α2 (A22), α4 (V74, A77, R78), α5 (V103, A106), and β3 (D110, K111, V112) (Figure 3). While the overall solvent-accessible surface area (SASA) of the polymorphic site was similar in all simulations, residue 108 was more exposed to solvent in the 108M protein (Table 2). In addition, the larger methionine formed closer side-chain contacts with residues A22, A77, and R78 (Table 2, Figure 3). V108 appeared to pack well with V74 (α4) at all temperatures, while the average M108-(Cγ)−V74(Cγ1) distance increased with temperature (Table 2). The L108 contact distances were intermediate between those of V108 and M108 (Table 2). While most contact distances for V108, L108, and M108 within the polymorphic site averaged ∼4.5 Å, M108 showed greater variability in its interactions and appeared to be more sensitive to structural changes in nearby helices α2 and α4.

Snapshots of 108L, 108V, and 108M COMT structures from the final nanosecond of the 37 and 50 °C trajectories are shown in Figure 4. All proteins retained the overall SAM-dependent methyltransferase fold topology throughout the simulations. In general, both the 108V and 108L proteins remained more compact than 108M COMT. While both 108V and 108M COMT demonstrated deviations greater than 2 Å in the orientation of α6 from its starting position, this appeared to have a greater impact on the SAM binding site (E90, Q120, W143) of 108M COMT. At 37 °C, reorientation of α8 and the catalytic loop (residues 198−205) was more pronounced in the 108M protein. The catechol binding site is defined by catalytic residue E199 and the "gate-keeping" residues W38 and P174, which form a channel that probably aids in directing substrate orientation and binding (*13*). The W38 (Cγ)−P174 (Cγ) distance was ∼22 Å in 108M COMT simulations at 37 and 50 °C; in 108V COMT this distance increased from 20 Å at 37 °C to 25 Å at 50 °C (Table 1). While disruption of the catechol binding site was evident in all proteins at 50 °C, the greater expansion of 108M COMT

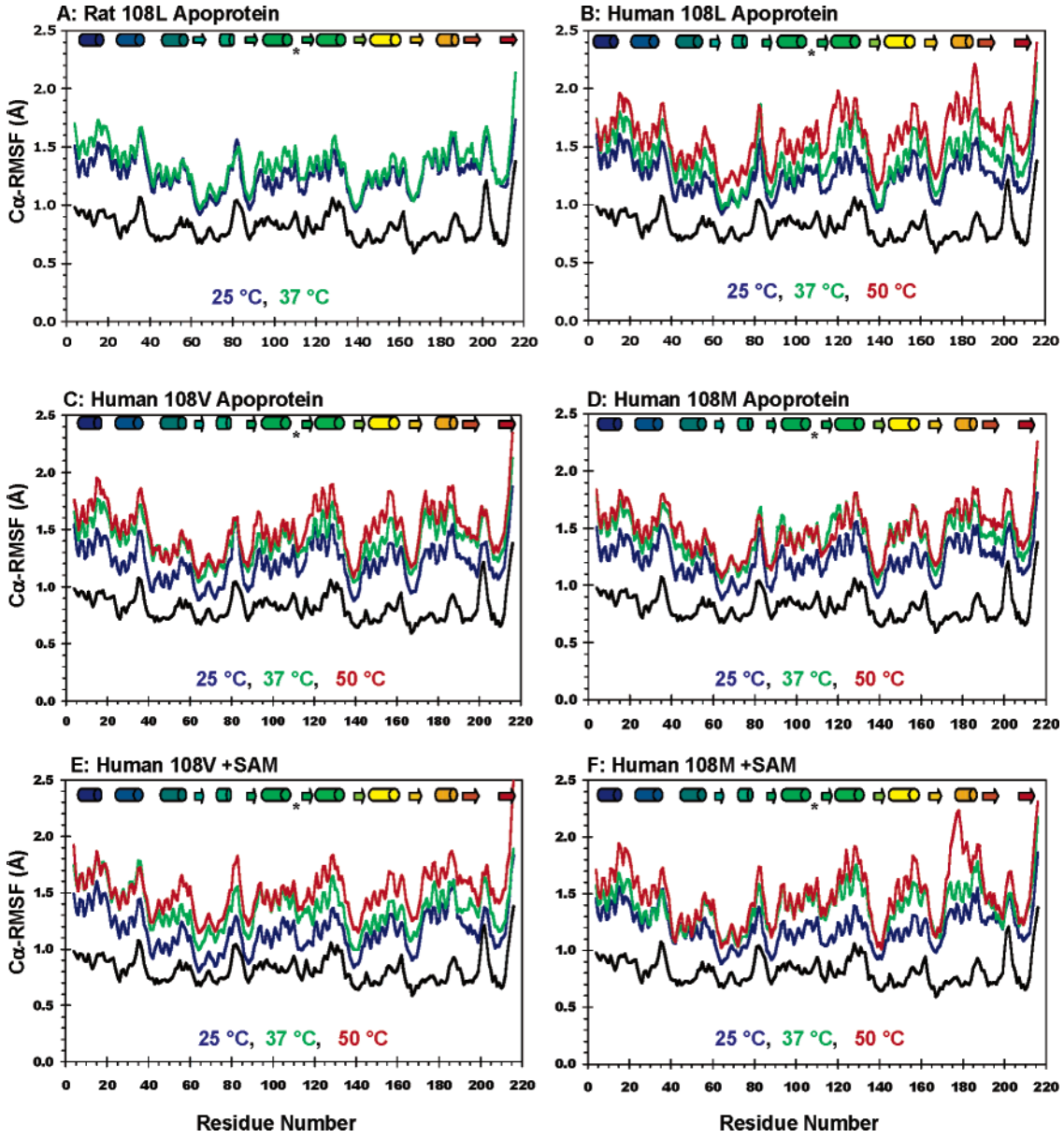

FIGURE 2: Cα-RMS fluctuations (in Å) per residue during the rat (1VID), 108L, 108V, and 108M MD simulations. Cα-RMSFs were calculated relative to the average structure over the last 10 ns of each simulation. Simulations at 25, 37, and 50 °C are colored in blue, green, and red, respectively. Crystallographic *B*-factors of holo rat COMT (1VID, *13*) are colored in black. Secondary structural elements are colored to match the representations of COMT in Figure 1. Key: cylinder, α-helix; arrow, *β*-strand; asterisk, residue 108.

appeared to increase this distortion. Overall, 108M COMT showed a larger distribution of disrupted structures at 37 °C, while active-site disorder was evident in the 108V and 108L proteins only at elevated temperatures.

The solvent-accessible surface area of the models was examined to investigate the effects of V108M-induced packing and structural changes on binding pocket conformations (Table 1, Figure 5). At 25 °C the average solvent accessibilities of the entire protein and the SAM and catechol binding sites were greater in 108M COMT than 108V COMT (Table 1). The solvent accessibility of the overall 108M protein was comparable at 37 and 50 °C, showing an increase of about 400 Å^2 at both temperatures relative to the 25 °C trajectories; a similar pattern was seen in the SAM binding site SASA (Table 1, Figure 5). The SASA of the catechol binding site remained constant at ∼900 Å^2. The active site expansion of 108V COMT appeared to lag behind that of the 108M protein. The SAM and catechol binding site solvent accessibilities of 108V COMT at 37 and 50 °C were comparable to those of 108M COMT at 25 and 37 °C, respectively (Table 1, Figure 5).

It has been suggested that the observed differences in COMT activity may reflect decreased protein levels in vivo. If this is the case, the recent finding of similar mRNA transcript levels for the two polymorphs in the dorsolateral prefrontal cortex suggests that the differences in COMT abundance result from altered protein degradation rates rather than differences in protein synthesis (*22*). The MD simulations suggest that all of the apoproteins sample a relatively small, distinct collection of conformations at 25 °C (Figure 6). A broader distribution of structures with increased Cα-RMSDs from the starting structure is present at 50 °C, although the overall topologies remain similar to those of the native protein (Figures 4 and 6). The MD simulations suggest that 108V COMT samples a smaller and more distinct collection of conformations at 37 °C (Figure 6). In

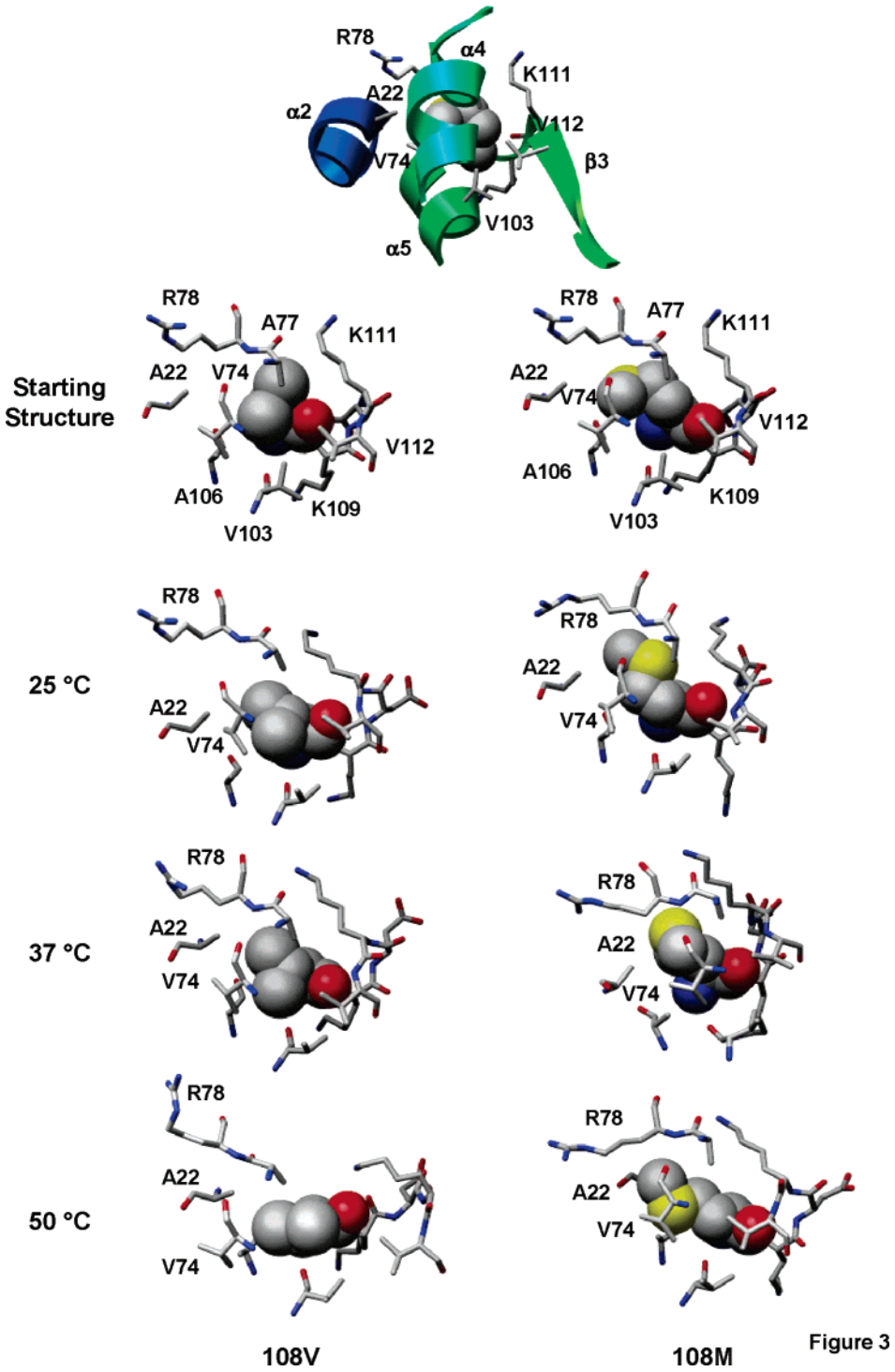

FIGURE 3: Snapshots of polymorphic packing taken from the initial structures and the 30th ns of the 25, 37, and 50 °C 108V and 108M apoprotein MD simulations. Residue 108 forms side-chain contacts with residues from α2 (A22), α4 (V74, A77, R78), α5 (V103, A106), and β3 (K109, D110, K111, V112). The larger M108 forms closer contacts at the polymorphic site. Residue 108 and residues lining the polymorphic site are shown in space-filling and licorice representations, respectively, and colored by atom. α-Helices and β-strands are colored to match the representations of COMT in Figure 1.

contrast, at 37 °C 108M COMT exists in a large ensemble of structures that overlap extensively with distorted conformations found at 50 °C (Figure 6).

Both 108V and 108M COMT appear to sample a larger distribution of structures of increased Cα-RMSD than 108L COMT at 37 °C, hinting that a leucine at position 108 may be stabilizing and that alterations in enzymatic activity may not be due solely to the size of residue 108. These differences suggest that 108M COMT's decreased activity may result from the presence of a larger proportion of inactive protein at physiological temperature. Furthermore, the overall expansion and increase in solvent accessibility of 108M COMT seen in the molecular dynamics simulations at physiological temperature could make 108M COMT more prone to enzymatic degradation.

Simulations of COMT with SAM. SAM has been found to protect the enzymatic activity of 108M COMT at both physiological and elevated temperatures (*8*). To examine the

Table 2: Polymorphic Site

		solvent-accessible surface area		residue 108 contact distance (Å)		
protein	temp (°C)	polymorphic site (Å^2)[a]	residue 108 (%)[b]	A22 (α2)[c]	V74 (α4)[d]	R78 (α4)[e]
108V apoprotein	initial	347	13.8	5.3	3.8	7.4
	25	452 ± 54	8.7 ± 3.6	4.2 ± 0.4	4.5 ± 0.4	6.5 ± 0.6
	37	420 ± 51	7.5 ± 3.3	4.2 ± 0.4	4.6 ± 0.5	6.7 ±0.5
	50	429 ± 58	6.8 ± 3.1	5.0 ± 0.5	4.4 ± 0.5	6.7 ±0.6
108M apoprotein	initial	359	11.4	4.3	6.6	5.4
	25	420 ± 69	19.7 ± 4.3	4.0 ± 0.4	4.5 ± 0.3	4.2 ± 0.4
	37	432 ± 65	18.0 ± 5.1	4.1 ± 0.5	4.9 ±0.6	4.5 ± 0.4
	50	430 ± 79	10.0 ± 5.6	4.9 ± 1.0	6.7 ± 0.7	6.2 ± 1.4
108L apoprotein	initial	372	10.3	4.2	4.3	4.6
	25	545 ± 68	28.0 ± 7.5	4.3 ± 0.5	4.8 ± 0.5	7.1 ± 0.5
	37	401 ± 53	10.5 ± 3.9	4.4 ± 0.4	5.0 ± 0.7	5.2 ±0.4
	50	417 ± 55	8.6 ± 3.9	4.2 ± 0.4	4.7 ± 0.6	5.3 ± 0.4
108V + SAM	initial	350	13.2	5.3	3.9	7.1
	25	440 ± 50	6.5 ± 2.7	4.5 ± 0.4	4.5 ± 0.4	6.4 ± 0.4
	37	422 ± 54	8.7 ± 3.6	4.4 ± 0.3	4.2 ± 0.3	6.0 ± 0.4
	50	432 ± 54	6.8 ± 3.0	4.4 ± 0.4	4.5 ± 0.4	5.8 ± 0.4
108M + SAM	initial	361	11.3	4.5	6.9	5.5
	25	465 ± 46	20.4 ± 4.2	3.8 ± 0.3	4.6 ± 0.3	5.0 ± 0.4
	37	463 ± 53	2.7 ± 1.6	5.0 ± 1.4	6.5 ± 0.4	6.8 ± 1.3
	50	478 ± 63	23.7 ± 6.2	4.1 ± 0.4	4.9 ± 0.7	5.2 ± 0.7

[a] The polymorphic site was defined using the following residues: A22, V74, A77, R78, V103, A106, 108, K109, D110, K111, and V112. Calculations used structures from the last 5 ns of each simulation. [b] The percent solvent exposure of residue 108 was calculated by dividing the side-chain exposure, averaged over the last 5 ns of each simulation, by the solvent accessibility of the side-chain free in solution. [c] Contact distances between the following atoms were averaged over the last 5 ns of each simulation: A22 (Cβ)−V108 (Cγ1), A22 (Cβ)−M108 (Cϵ), and A22 (Cβ)−L108 (Cδ1). [d] V74 (Cγ2)−V108 (Cγ2), V74 (Cγ1)−M108 (Cγ), and V74 (Cγ2)−L108 (Cδ1). [e] Contact distances between the following atoms were averaged over the last 5 ns of each simulation: R78 (Cβ)−V108 (Cγ1), R78 (Cβ)−M108 (Cϵ), and R78 (Cβ)−L108 (Cδ2).

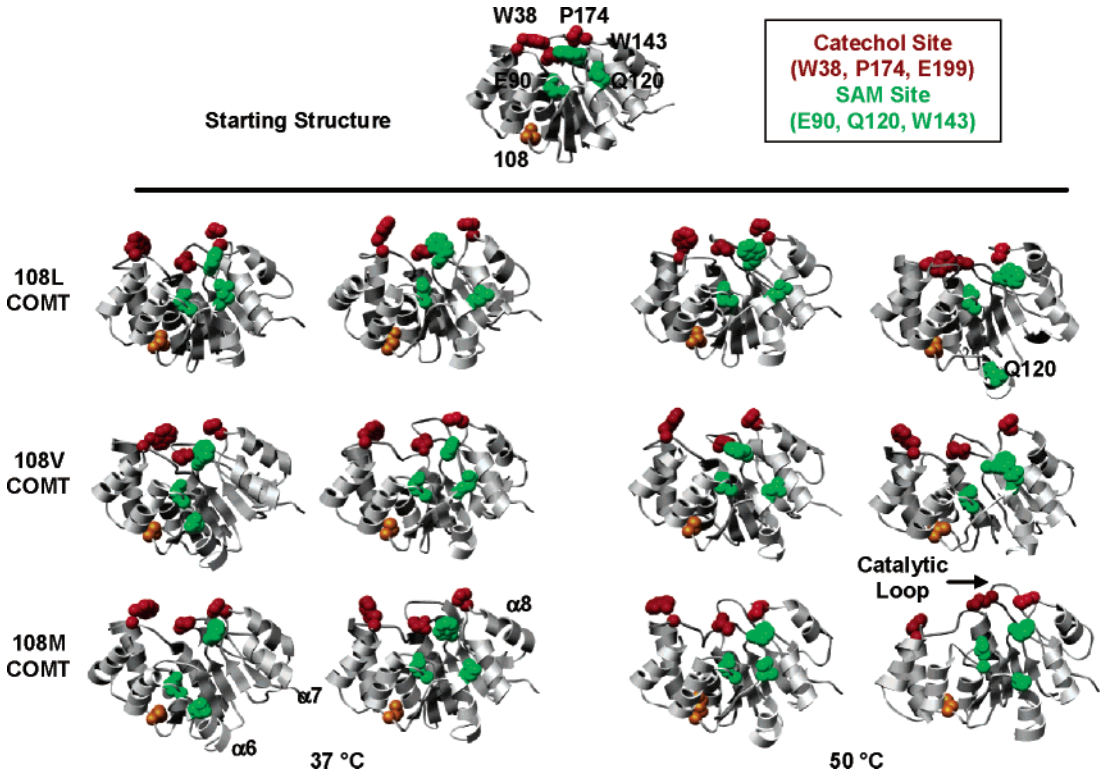

FIGURE 4: The 108M COMT active site is disposed to disruption at 37 °C. Snapshots from the 30th ns each of the 37 and 50 °C apoprotein MD simulations (i.e., two simulations at each temperature) are shown as ribbon representations. SAM binding residues E90, Q120, and W143 are colored in green, and catechol binding residues W38, P174, and E199 are colored in red. Residue 108 is colored in orange.

interactions between COMT and SAM that contribute to this stabilizing effect, we performed simulations of both 108V and 108M COMT with SAM bound to the active site. SAM remained bound to COMT throughout all of the simulations. The presence of SAM had no significant effect on the overall solvent accessibility of the polymorphic site or residue 108 (Table 2). Variability in contact distances within the polymorphic site decreased within individual simulations. Inter-

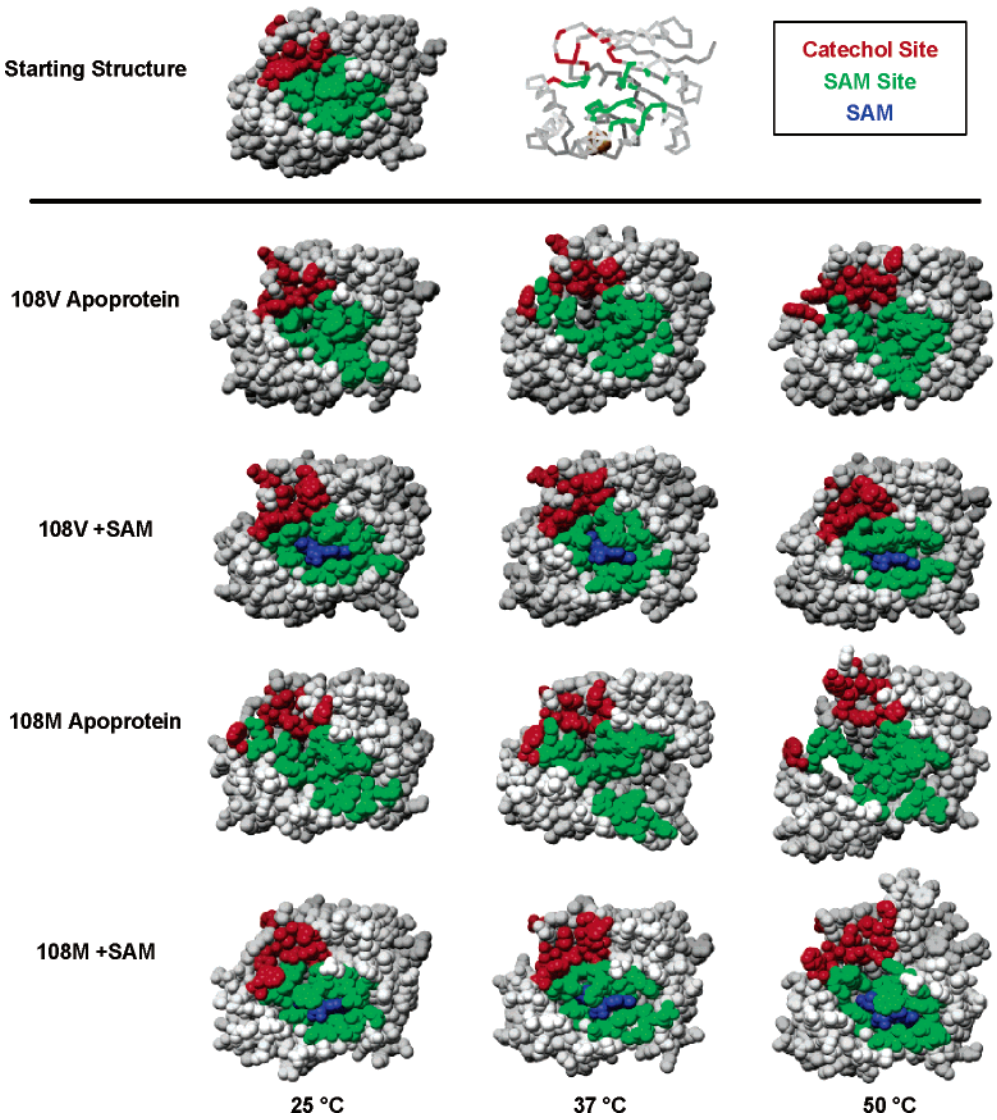

FIGURE 5: Space-filling representations of COMT showing increasing solvent exposure of the SAM binding site with temperature. The 108M COMT active site is more exposed to solvent. Residues forming the SAM and catechol binding sites are colored in green and red, respectively. SAM is colored in blue.

estingly, the M108 (Cϵ)−R78 (Cβ) contact distance increased in the SAM simulations, becoming comparable to that of the 108V protein (Table 2).

The addition of SAM to 108V COMT decreased the total Cα-RMSD of the trajectories to ∼1.8 Å at all temperatures (Table 1). A similar decrease in Cα-RMSD was seen in 108M COMT at 37 °C. The Cα-RMSFs of residues 65−140 were lower in both proteins with SAM bound than those of the apoprotein (Figure 2E,F). This was expected as helices α3−α6 contain many SAM binding residues (Figure 1). The addition of SAM also resulted in decreased Cα-RMSFs for α1−α3 and the catalytic loop of 108M COMT at 37 °C (Figure 2D,F). However, SAM did not have a stabilizing effect on 108M COMT in the 50 °C trajectory, which reached a final Cα-RMSD of 3.8 ± 0.1 Å and displayed increased fluctuations in both the amino (α1−α2) and carboxy termini [α7−α8, catalytic loop (residues 198−205)] (Table 1, Figure 2F).

The addition of SAM to both 108V and 108M COMT significantly decreased the solvent accessibilities of the overall protein and the SAM binding site at 25 and 37 °C (Table 1, Figure 5). However, in the 50 °C simulation of 108M COMT with SAM, the total and catechol binding site SASAs increased (Table 1, Figure 5). This was consistent with the increase in Cα-RMSF for the amino- and carboxy-terminal regions of 108M COMT (Figure 2F). While both proteins maintained most of the key SAM contact distances at 37 °C, some residues lining the SAM binding pocket of 108M COMT, particularly M40, S72, and S119, did not interact as well with SAM at 50 °C (Supporting Information, Table S2). In the crystal structures of the rat protein, as well as the simulations described here, M40, V42, and S72 interact with the methionine moiety of SAM near the catechol binding pocket (*13*−*15*). M40 orients the sulfur of SAM toward the hydroxyl groups of the catechol substrate.

In addition, while D141 maintains hydrogen bond with SAM during the simulation of 108M COMT at 50 °C, an important contact between D141 and K144 is lost. D141 is involved in coordinating the Mg^{2+} cofactor. Mg^{2+} helps to orient the catechol substrate hydroxyl groups for methyl transfer, while K141 probably aids in proton abstraction from the catechol hydroxyl group (*13*, *60*, *62*). SAM binding also decreased the W38−P174 contact distance in both proteins at physiological temperature (Table 1). However, stabilization

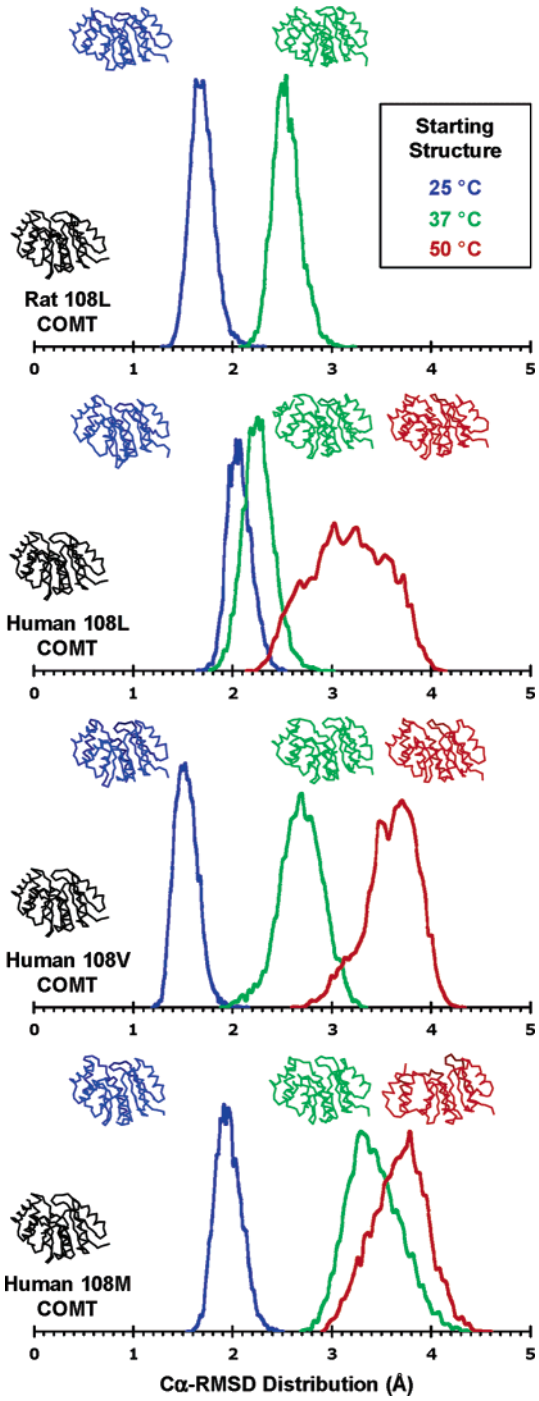

FIGURE 6: Distributions of total Cα-RMSD (Å) during the last 10 ns of rat COMT and human 108L, 108V, and 108M COMT simulations at 25, 37, and 50 °C. At 37 °C, 108M COMT exists in a large ensemble of structures that overlap extensively with distorted conformations found at 50 °C. The distribution of structures is smaller and more distinct in the 108V COMT simulations, particularly at 37 °C. These differences suggest that 108M COMT's decreased activity may result from the presence of a larger proportion of inactive protein at physiological temperature. Structures are colored in black (starting structure), blue (25 °C), green (37 °C), and red (50 °C).

of the W38−P174 interaction was not observed in 108M COMT at 50 °C. The simulations indicate that although SAM binding may protect COMT's overall structure at 50 °C, partial rearrangements of the SAM and catechol binding sites occur in 108M COMT at elevated temperature independent of the presence of SAM.

CONCLUSIONS

Several of the differences in the behavior of 108V and 108M COMT in our MD trajectories could be important for enzymatic activity. Replacing valine 108 with methionine increased the solvent exposure of residue 108 and had significant effects on tertiary contacts between secondary structural elements α2, α4, and α5 in the immediate vicinity of this residue. While both proteins retained the overall methyltransferase fold topology at all temperatures studied, the simulations suggest that 108M COMT exists in a broader ensemble of conformational states at 37 °C than 108V COMT. Perhaps most importantly, 108M COMT was more prone to deformation at physiological temperatures, with large increases in total and SAM binding site solvent accessibility. Similar structural perturbations were observed in both proteins at 50 °C, a temperature close to their respective T_{50} values. These results indicate that a larger proportion of 108M COMT may exist in deformed, and thus possibly inactive, conformations at 37 °C. The addition of SAM resulted in decreases in both the overall and SAM binding site solvent accessibilities and reduced the Cα-RMS fluctuations of both proteins at physiological temperatures. This stabilizing effect of SAM may explain the protective effects of SAM on 108M COMT activity.

ACKNOWLEDGMENT

Molecular graphics images were produced using the UCSF Chimera package from the Computer Graphics Laboratory, University of California, San Francisco (supported by NIH Grant P41 RR-01081) (*77*).

SUPPORTING INFORMATION AVAILABLE

Force-field parameters for the SAM model (Table S1) and side-chain contact distances reflecting SAM binding (Table S2). This material is available free of charge via the Internet at http://pubs.acs.org.

REFERENCES

1. Axelrod, J., and Tomchick, R. (1958) Enzymatic O-methylation of epinephrine and other catechols, *J. Biol. Chem. 233*, 702−705.
2. Männistö, P. T., and Kaakkola, S. (1999) Catechol-*O*-methyltransferase (COMT): biochemistry, molecular biology, pharmacology, and clinical efficacy of the new selective COMT inhibitors, *Pharmacol. Rev. 51*, 593−628.
3. Bonifati, V., and Meco, G. (1999) New, selective catechol-*O*-methyltransferase inhibitors as therapeutic agents in Parkinson's disease, *Pharmacol. Ther. 81*, 1−36.
4. Grossman, M. H., Emanueal, B. S., and Budarf, M. L. (1992) Chromosomal mapping of the human catechol-*O*-methyltransferase gene to 22q11.1-q11.2, *Genomics 12*, 822−825.
5. Lundstrom, K., Salminen, M., Jalanko, A., Savolainen, K., and Ulmanen, I. (1995) Cloning, expression and structure of catechol-*O*-methyltransferase, *Biochim. Biophys. Acta 1251*, 1−10.
6. Tenhunen, J., Salminen, M., Jalanko, A., Ukkonen, S., and Ulmanen, I. (1993) Structure of the rat catechol-*O*-methyltransferase gene: separate promoters are used to produce mRNAs for soluble and membrane-bound forms of the enzyme, *DNA Cell Biol. 12*, 253−263.
7. Tenhunen, J., Salminen, M., Lundstrom, K., Kiviluoto, T., Savolainen, R., and Ulmanen, I. (1994) Genomic organization of the human catechol *O*-methyltransferase gene and its expression from two distinct promoters, *Eur. J. Biochem. 223*, 1049−1059.
8. Lotta, T., Vidgren, J., Tilgmann, C., Ulmanen, I., Melen, K., Julkunen, I., and Taskinen, J. (1995) Kinetics of human soluble and membrane-bound catechol *O*-methyltransferase: a revised

mechanism and description of the thermolabile variant of the enzyme, *Biochemistry 34*, 4202−4210.
9. Rivett, A. J., Francis, A., and Roth, J. A. (1983) Distinct cellular localization of membrane-bound and soluble forms of catechol-*O*-methyltransferase in brain, *J. Neurochem. 40*, 215−219.
10. Rivett, A. J., Francis, A., and Roth, J. A. (1983) Localization of membrane-bound catechol-*O*-methyltransferase, *J. Neurochem. 40*, 1494−1496.
11. Cheng, X., and Roberts, R. J. (2001) AdoMet-dependent methylation, DNA methyltransferases and base flipping, *Nucleic Acids Res. 29*, 3784−3795.
12. Martin J. L., and McMillan F. M. (2002) SAM (dependent) I AM: the *S*-adenosylmethionine-dependent methyltransferase fold, *Curr. Opin. Struct. Biol. 12*, 783−793.
13. Vidgren, J., Svensson, L. A., and Liljas, A. (1994) Crystal structure of catechol *O*-methyltransferase, *Nature 368*, 354−358.
14. Lerner, C., Ruf, A., Gramlich, V., Masjost, B., Zurcher, G., Jakob-Roetne, R., Borroni, E., and Diederich, F. (2001) X-ray crystal structure of a bisubstrate inhibitor bound to the enzyme catechol-*O*-methyltransferase: a dramatic effect of inhibitor preorganization on binding affinity, *Angew. Chem., Int. Ed. Engl. 40*, 4040−4042.
15. Bonifacio, M. J., Archer, M., Rodrigues, M. L., Matias, P. M., Learmonth, D. A., Carrondo, M. A., and Soares-Da-Silva, P. (2002) Kinetics and crystal structure of catechol-*O*-methyltransferase complex with co-substrate and a novel inhibitor with potential therapeutic application, *Mol. Pharmacol. 62*, 795−805.
16. Bertocci, B., Miggiano, V., Da Prada, M., Dembic, Z., Lahm, H. W., and Melherbe, P. (1991) Human catechol-*O*-methyltransferase: cloning and expression of the membrane-associated form, *Proc. Natl. Acad. Sci. U.S.A. 88*, 1416−1420.
17. Lundstrom, K., Tenhunen, J., Tilgmann, C., Karhunen, T., Panula, P., and Ulmanen, I. (1995) Cloning, expression and structure of catechol-*O*-methyltransferase, *Biochim. Biophys. Acta 1251*, 1−10.
18. Lachman, H. M., Papolos, D. F., Saito, T., Yu, Y. M., Szumlanski, C. L., and Weinshilboum, R. M. (1996) Human catechol-*O*-methyltransferase pharmacogenetics: description of a functional polymorphism and its potential application to neuropsychiatric disorders, *Pharmacogenetics 6*, 243−250.
19. Weinshilboum, R. M., and Raymond, F. A. (1977) Inheritance of low erythrocyte catechol-*O*-methyltransferase activity in man, *Am. J. Hum. Genet. 29*, 125−135.
20. Palmatier, M. A., Kang, A. M., and Kidd, K. K. (1999) Global variation in the frequencies of functionally different catechol-*O*-methyltransferase alleles, *Biol. Psychiatry 46*, 557−567.
21. Goodman, J. E., Jensen, L. T., He, P., and Yager, J. D. (2002) Characterization of human soluble high and low activity catechol-*O*-methyltransferase catalyzed catechol estrogen methylation, *Pharmacogenetics 12*, 517−528.
22. Chen, J., Lipska, B. K., Halim, N., Ma, Q. D., Matsumoto, M., Melhem, S., Kolachana, B. S., Hyde, T. M., Herman, M. M., Apud, J., Egan, M. F., Kleinman, J. E., and Weinberger, D. R. (2004) Functional analysis of genetic variation in catechol-*O*-methyltransferase (*COMT*): effects on mRNA, protein, and enzyme activity in postmortem human brain, *Am. J. Hum. Genet. 75*, 807−821.
23. Scanlon, P. D., Raymond, F. A., and Weinshilboum, R. M. (1979) Catechol-*O*-methyltransferase: thermolabile enzyme in erythrocytes of subjects homozygous for allele for low activity, *Science* 203, 63−65.
24. Spielman, R. S., and Weinshilboum, R. M. (1981) Genetics of red cell COMT activity: analysis of thermal stability and family data, *Am. J. Med. Genet. 10*, 279−290.
25. Boudikova, B., Szumlanski, C., Maidak, B., and Weinshilboum, R. (1990) Human liver catechol-*O*-methyltransferase pharmacogenetics, *Clin. Pharmacol. Ther. 48*, 381−389.
26. Grossman, M. H., Szumlanski, C., Littrell, J. B., Weinstein, R., and Weinshilboum, R. M. (1992) Electrophoretic analysis of low and high activity forms of catechol-*O*-methyltransferase in human erythrocytes, *Life Sci. 50*, 473−480.
27. Aksoy, S., Klener, J., and Weinshilboum, R. M. (1993) Catechol *O*-methyltransferase pharmacogenetics: photoaffinity labeling and western blot analysis of human liver samples, *Pharmacogenetics 3*, 116−122.
28. Shield, A. J., Thomae, B. A., Eckloff, B. W., Wieben, E. D., and Weinshilboum, R. M. (2004) Human catechol *O*-methyltransferase genetic variation: gene resequencing and functional characterization of variant allozymes, *Mol. Psychiatry 9*, 151−160.
29. Weinshilboum, R., and Dunnette, J. (1981) Thermal stability and the biochemical genetics of erythrocyte catechol-*O*-methyltransferase and plasma dopamine-beta-hydroxylase, *Clin. Genet. 19*, 426−437.
30. Syvanen, A. C., Tilgmann, C., Rinne, J., and Ulmanen, I. (1997) Genetic polymorphism of catechol-*O*-methyltransferase (COMT): correlation of genotype with individual variation of S-COMT activity and comparison of the allele frequencies in the normal population and parkinsonian patients in Finland, *Pharmacogenetics 7*, 65−71.
31. Cotton, N. J, Stoddard, B., and Parson, W. W. (2004) Oxidative inhibition of human soluble catechol *O*-methyltransferase, *J. Biol. Chem. 279*, 23710−23718.
32. Li, Y., Yang, X., Chang, M., Yager, J. D., van Breeman, R. B., and Bolton, J. L. (2005) Functional and structural comparisons of cysteine residues in the Val108 wild type and Met108 variant of human soluble catechol *O*-methyltransferase, *Chem.-Biol. Interact. 152*, 151−163.
33. Bray, N. J., Buckland, P. R., Williams, N. M, Williams, H. J, Norton, N., Owen, M. J., and O'Donovan, M. C. (2003) A haplotype implicated in schizophrenia susceptibility is associated with reduced COMT expression in human brain, *Am. J. Hum. Genet. 73*, 152−161.
34. Zhu, G., Lipsky, R. H., Xu, K., Ali, S., Hyde, T., Kleinman, J., Akhtar, L. A., Mash, D. C., and Goldman, D. (2004) Differential expression of human COMT alleles in brain and lymphoblasts detected by RT-coupled 5′ nuclease assay, *Psychopharmacology 177*, 178−184.
35. Dawling, S., Roodi, N., Mernaugh, R. L., Wang, X., and Parl, F. F. (2001) Catechol-*O*-methyltransferase (COMT)-mediated metabolism of catechol estrogens: comparison of wild-type and variant COMT isoforms, *Cancer Res. 61*, 6716−6722.
36. Yim, D. S., Park, S. K., Yoo, K. Y., Yoon, K. S., Chung, H. H., Kang, H. L., Ahn, S. H., Noh, D. Y., Choe, K. J., Jang, I. J., Shin, S. G., Strickland, P. T., Hirvonen, A., and Kang, D. (2001) Relationship between the Val158Met polymorphism of catechol *O*-methyltransferase and breast cancer, *Pharmacogenetics 11*, 279−286.
37. Wedren, S., Rudqvist, T. R., Granath, F., Weiderpass, E., Ingelman-Sundberg, M., Persson, I., and Magnusson, C. (2003) Catechol-*O*-methyltransferase gene polymorphism and postmenopausal breast cancer risk, *Carcinogenesis 24*, 681−687.
38. Karayiorgou, M., Altemus, M., Galke, B. L., Goldman, D., Murphy, D. L., Ott, J., and Gogos, J. A. (1999) Genotype determining low catechol-*O*-methyltransferase activity as a risk factor for obsessive-compulsive disorder, *Proc. Natl. Acad. Sci. U.S.A. 94*, 4572−4574.
39. Li, T., Vallada, H., Curtis, D., Arranz, M., Xu, K., Cai, G., Deng, H., Liu, J., Murray, R., Liu, X., and Collier, D. A. (1997) Catechol-*O*-methyltransferase Val158Met polymorphism: frequency analysis in Han Chinese subjects and allelic association of the low activity allele with bipolar affective disorder, *Pharmacogenetics 7*, 349−353.
40. Kirov, G., Murphy, K. C., Arranz, M. J., Jones, I., McCandles, F., Kunigi, H., Murray, R. M., McGuffin, P., Collier, D. A., Owen, M. J., and Craddock, N. (1998) Low activity allele of catechol-*O*-methyltransferase gene associated with rapid cycling bipolar disorder, *Mol. Psychiatry 3*, 342−345.
41. Papolos, D. F., Veit, S., Faedda, G. L., Saito, T., and Lachman, H. M. (1998) Ultra-ultra rapid cycling bipolar disorder is associated with the low activity catecholamine-*O*-methyltransferase allele, *Mol. Psychiatry 3*, 346−349.
42. Tiihonen, J., Hallikainen, T., Lachman, H., Saito, T., Volavka, J., Kauhanen, J., Salonen, J. T., Ryynanen, O. P., Koulu, M., Karvonen, M. K., Pohjalainen, T., Syvalahti, E., and Hietala, J. (1999) Association between the functional variant of the catechol-*O*-methyltransferase (COMT) gene and type 1 alcoholism, *Mol. Psychiatry 4*, 286−289.
43. Kauhanen, J., Hallikainen, T., Tuomainen, T. P., Koulu, M., Karvonen, M. K., Salonen, J. T., and Tiihonen, J. (2000) Association between the functional polymorphism of catechol-*O*-methyltransferase gene and alcohol consumption among social drinkers, *Alcohol Clin. Exp. Res. 24*, 135−139.
44. Wang, T., Franke, P., Neidt, H., Cichon, S., Knapp, M., Lichtermann, D., Maier, W., Propping, P., and Nothen, M. M. (2001) Association study of the low-activity allele of catechol-*O*-methyltransferase and alcoholism using a family based approach, *Mol. Psychiatry 6*, 109−111.

45. Strous, R. D., Bark, N., Parsia, S. S., Volavka, J., and Lachman, H. M. (1997) Analysis of a functional catechol-*O*-methyltransferase gene polymorphism in schizophrenia: evidence for association with aggressive and antisocial behavior, *Psychiatry Res. 69*, 71−77.
46. Lachman, H. M., Nolan, K. A., Mohr, P., Saito, T., and Volavka, J. (1998) Association between catechol *O*-methyltransferase genotype and violence in schizophrenia and schizoaffective disorder, *Am. J. Psychiatry 155*, 835−837.
47. Kotler, M., Barak, P., Cohen, H., Averbuch, I. E., Grinshpoon, A., Gritsenko, I., Nemanov, L., and Ebstein, R. P. (1999) Homicidal behavior in schizophrenia associated with a genetic polymorphism determining low catechol *O*-methyltransferase (COMT) activity, *Am. J. Med. Genet. 88*, 628−633.
48. Nolan, K. A., Volavka, J., Czobor, P., Cseh, A., Lachman, H., Saito, T., Tiihonen, J., Putkonen, A., Hallikainen, T., Kotilainen, I., Rasanen, P., Isohanni, M., Jarvelin, M. R., and Karvonen, M. K. (2000) Suicidal behavior in patients with schizophrenia is related to COMT polymorphism, *Psychiatr. Genet. 10*, 117−124.
49. Strous, R. D., Nolan, K. A., Lapidus, R., Diaz, L., Saito, T., and Lachman, H. M. (2003) Aggressive behavior in schizophrenia is associated with the low enzyme activity COMT polymorphism: a replication study, *Am. J. Med. Genet., B: Neuropsychiatr. Genet. 120*, 29−34.
50. Shifman, S., Bronstein, M., Sternfeld, M., Pisante-Shalom, A., Lev-Lehman, E., Weizman, A., Reznik, I., Spivak, B., Grisaru, N., Karp, L., Schiffer, R., Kotler, M., Strous, R. D., Swartz-Vanetik, M., Knobler, H. Y., Shinar, E., Beckmann, J. S., Yakir, B., Risch, N., Zak, N. B., and Darvasi, A. (2002) A highly significant association between a COMT haplotype and schizophrenia, *Am. J. Hum. Genet. 71*, 1296−1302.
51. Shifman, S., Bronstein, M., Sternfeld, M., Pisante, A., Weizman, A., Reznik, I., Spivak, B., Grisaru, N., Karp, L., Schiffer, R., Kotler, M., Strous, R. D., Swartz-Vanetik, M., Knobler, H. Y., Shinar, E., Yakir, B., Zak, N. B., and Darvasi, A. (2004) COMT: a common susceptibility gene in bipolar disorder and schizophrenia, *Am. J. Med. Genet., B: Neurophsychiatr. Genet. 128*, 61−64.
52. Horowitz, A., Shifman, S., Rivlin, N., Pisante, A., Darvasi, A. (2005) Further tests of the association between schizophrenia and single nucleotide polymorphism markers at the catechol-*O*-methyltransferase locus in an Askenazi Jewish population using microsatellite markers, *Psychiatr. Genet. 15*, 163−169.
53. Lachman, H. M., Morrow, B., Shprintzen, R., Veit, S., Parsia, S. S., Faedda, G., Goldberg, R., Kucherlapati, R., and Papolos, D. F. (1996) Association of codon 108/158 catechol-*O*-methyltransferase gene polymorphism with the psychiatric manifestations of velo-cardio-facial syndrome, *Am. J. Med. Genet. 67*, 468−472.
54. Graf, W. D., Unis, A. S., Yates, C. M., Sulzbacher, S., Dinulos, M. B., Jack, R. M., Dugaw, K. A., Paddock, M. N., and Parson, W. W. (2001) Catecholamines in patients with 22q11.2 deletion syndrome and the low-activity COMT polymorphism, *Neurology 57*, 410−416.
55. Scambler, P. J. (2000) The 22q11 deletion syndromes, *Hum. Mol. Genet. 9*, 2421−2426.
56. Zubieta, J.-K., Heitzeg, M. M., Smith, Y. R., Bueller, J. A., Xu, K., Xu, Y., Koeppe, R. A., Stohler, C. S., Goldman, D. (2003) COMT val158met genotype affects μ-opioid neurotransmitter responses to a pain stressor, *Science 299*, 1240−1243.
57. Diatchenko, L., Slade, G. D., Nackley, A. G., Bhalang, K., Sigurdsson, A., Belfer, I., Goldman, D., Xu, K., Shabalina, S. A., Shagin, D., Max, M. B., Makarov, S. S., and Maixner, W. (2005) Genetic basis for individual variations in pain perception and the development of a chronic pain condition, *Hum. Mol. Genet. 14*, 135−143.
58. Goldberg, T. E., and Weinberger, D. R. (2004) Genes and the parsing of cognitive processes, *Trends Cognit. Sci. 8*, 325−335.
59. Meyer-Lindenberg, A., Kohn, P. D., Kolachana, B., Kippenhan, S., McInerney-Leo, A., Nussbaum, R., Weinberger, D. R., Berman, K. F. (2005) Midbrain dopamine and prefrontal function in humans: interaction and modulation by *COMT* genotype, *Nat. Neurosci. 8*, 594−596.
60. Zheng, Y. J., and Bruice, T. C. (1997) A theoretical examination of the factors controlling the catalytic efficiency of a transmethylation enzyme: catechol-*O*-methyltransferase, *J. Am. Chem. Soc. 119*, 8137−8145.
61. Lau, E. Y., and Bruice, T. C. (1998) Importance of correlated motions in forming highly reactive near attack conformations in catechol *O*-methyltransferase, *J. Am. Chem. Soc. 120*, 12387−12394.
62. Kuhn, B., and Bruice, T. C. (2000) Transition-state and ground-state structures and their interaction with the active-site residues in catechol *O*-methyltransferase, *J. Am. Chem. Soc. 122*, 46−51.
63. Yau, E. Y., and Bruice, T. C. (2000) Comparison of the dynamics for ground-state and transition-state structures in the active site of catechol-*O*-methyltransferase, *J. Am. Chem. Soc. 122*, 7165−7171.
64. Kuhn, B., and Kollman, P. A. (2000) QM-FE and molecular dynamics calculations on catechol-*O*-methyltransferase: free energy of activation in the enzyme and in aqueous solution and regioselectivity of the enzyme-catalyzed reaction, *J. Am. Chem. Soc. 122*, 2586−2596.
65. Kollman, P. A., Kuhn, B., Donini, O., Perakyla, M., Stanton, R., and Bakowies, D. (2001) Elucidating the nature of enzyme catalysis utilizing a new twist on an old methodology: quantum mechanical-free energy calculations on chemical reactions in enzymes and in aqueous solution, *Acc. Chem. Res. 34*, 72−79.
66. Roca, M., Marti, S., Andres, J., Moliner, V., Tunon, I., Bertran, J., and Williams, I. H. (2003) Theoretical modeling of enzyme catalytic power: analysis of "cratic" and electrostatic factors in catechol-*O*-methyltransferase, *J. Am. Chem. Soc. 125*, 7726−7737.
67. Alden, R. G., Parson, W. W., Chu, Z. T., and Warshel, A. (1996) Orientation of the OH dipole of tyrosine (M)210 and its effect on electrostatic energies in photosynthetic bacterial reaction centers, *J. Phys. Chem. 100*, 16761−16770.
68. Levitt, M., Hirshberg, M., Sharon, R., and Daggett, V. (1995) Potential energy function and parameters for simulations of the molecular dynamics of proteins and nucleic acids in solution, *Comput. Phys. Commun. 91*, 215−231.
69. Beck, D. A. C., Alonso, D. O. V., and Daggett, V. (2004) *il*mm, computer program, *in lucem* Molecular Mechanics, University of Washington, Seattle, WA.
70. Levitt, M. (1990) ENCAD, computer program, Energy Calculations and Dynamics, Molecular Applications Group, Palo Alto, CA, and Yeda, Rehovot, Israel.
71. Levitt, M., Hirshberg, M., Sharon, R., Laidig, K. E., and Daggett, V. (1997) Calibration and testing of a water model for simulation of the molecular dynamics of proteins and nucleic acids in solution, *J. Phys. Chem. B 101*, 5051−5061.
72. Beck, D. A. C., and Daggett, V. (2004) Methods for molecular dynamics simulations of protein folding/unfolding in solution, *Methods 34*, 112−120.
73. Kell, G. S. (1967) Precise representation of volume properties of water at one atmosphere, *J. Chem. Eng. Data 12*, 66−69.
74. Huang, X., and Miller, W. (1991) A time-efficient, linear-space local similarity algorithm, *Adv. Appl. Math. 12*, 337−357.
75. Hubbard, S. J., and Thorton, J. M. (1993) NACCESS Computer Program, Department of Biochemistry and Molecular Biology, University College, London.
76. Hünenberger, P. H., Mark, A. E., and van Gunsteren, W. F. (1995) Fluctuation and cross-correlation analysis of protein motions observed in nanosecond molecular dynamics simulations, *J. Mol. Biol. 252*, 492−503.
77. Pettersen, E. F., Goddard, T. D., Huang, C. C., Couch, G. S., Greenblatt, D. M., Meng, E. C., and Ferrin, T. E. (2004) UCSF Chimera−a visualization system for exploratory research and analysis, *J. Comput. Chem. 25*, 1605−1612.

BI051988I